AFRL-ML-WP-TP-2006-425

A STUDY OF THE FORMATION, PURIFICATION, LIGAND SUBSTITUTION CHEMISTRY, AND APPLICATION AS A SWNT GROWTH CATALYST OF THE NANOCLUSTER (PREPRINT)

Robin E. Anderson, Ramon Colorado, Jr., Christopher Crouse, Douglas Ogrin, Christopher L. Edwards, Elizabeth Whitsitt, Valerie C. Moore, Dorothy Koveal, Corina Lupu, Michael Stewart, Richard E. Smalley, James M. Tour, Andrew R. Barron, Benji Maruyama, and Mark J. Pender

FEBRUARY 2006

MATERIALS AND MANUFACTURING DIRECTORATE
AIR FORCE RESEARCH LABORATORY
AIR FORCE MATERIEL COMMAND
WRIGHT-PATTERSON AIR FORCE BASE, OH 45433-7750

NOTICE AND SIGNATURE PAGE

Using Government drawings, specifications, or other data included in this document for any purpose other than Government procurement does not in any way obligate the U.S. Government. The fact that the Government formulated or supplied the drawings, specifications, or other data does not license the holder or any other person or corporation; or convey any rights or permission to manufacture, use, or sell any patented invention that may relate to them.

This report was cleared for public release by the Air Force Research Laboratory Wright Site (AFRL/WS) Public Affairs Office and is available to the general public, including foreign nationals. Copies may be obtained from the Defense Technical Information Center (DTIC) (http://www.dtic.mil).

AFRL-ML-WP-TP-2006-425 HAS BEEN REVIEWED AND IS APPROVED FOR PUBLICATION IN ACCORDANCE WITH ASSIGNED DISTRIBUTION STATEMENT.

*//Signature//

BENJI MARUYAMA, Program Manager
Structural Materials Branch
Nonmetallic Materials Division

//Signature//

TIA BENSON TOLLE, Chief
Structural Materials Branch
Nonmetallic Materials Division

//Signature//

SHASHI K. SHARMA, Acting Deputy Chief
Nonmetallic Materials Division
Materials and Manufacturing Directorate

This report is published in the interest of scientific and technical information exchange, and its publication does not constitute the Government's approval or disapproval of its ideas or findings.

*Disseminated copies will show "//Signature//" stamped or typed above the signature blocks.

REPORT DOCUMENTATION PAGE

Form Approved
OMB No. 0704-0188

1. REPORT DATE *(DD-MM-YY)*	2. REPORT TYPE	3. DATES COVERED *(From - To)*
February 2006	Journal Article Preprint	

4. TITLE AND SUBTITLE

A STUDY OF THE FORMATION, PURIFICATION, LIGAND SUBSTITUTION CHEMISTRY, AND APPLICATION AS A SWNT GROWTH CATALYST OF THE NANOCLUSTER (PREPRINT)

5a. CONTRACT NUMBER
In-house

5b. GRANT NUMBER

5c. PROGRAM ELEMENT NUMBER
N/A

6. AUTHOR(S)

Robin E. Anderson, Ramon Colorado, Jr., Christopher Crouse, Douglas Ogrin, Christopher L. Edwards, Elizabeth Whitsitt, Valerie C. Moore, Dorothy Koveal, Corina Lupu, Michael Stewart, Richard E. Smalley, James M. Tour, and Andrew R. Barron (Rice University)
Benji Maruyama, and Mark J. Pender (AFRL/MLBC)

5d. PROJECT NUMBER
N/A

5e. TASK NUMBER
N/A

5f. WORK UNIT NUMBER
M03R1000

7. PERFORMING ORGANIZATION NAME(S) AND ADDRESS(ES)

Rice University
Department of Chemistry and
Center for Nanoscale
Science and Technology
Houston TX 77005

Structural Materials Branch (AFRL/MLBC)
Nonmetallic Materials Division
Materials and Manufacturing Directorate
Air Force Research Laboratory, Air Force Materiel Command
Wright-Patterson Air Force Base, OH 45433-7750

8. PERFORMING ORGANIZATION REPORT NUMBER

9. SPONSORING/MONITORING AGENCY NAME(S) AND ADDRESS(ES)

Materials and Manufacturing Directorate
Air Force Research Laboratory
Air Force Materiel Command
Wright-Patterson AFB, OH 45433-7750

10. SPONSORING/MONITORING AGENCY ACRONYM(S)
AFRL-ML-WP

11. SPONSORING/MONITORING AGENCY REPORT NUMBER(S)
AFRL-ML-WP-TP-2006-425

12. DISTRIBUTION/AVAILABILITY STATEMENT
Approved for public release; distribution is unlimited.

13. SUPPLEMENTARY NOTES
This paper was submitted to the Dalton Transactions Royal Society of Chemistry.
This paper contains color. PAO Case Number: AFRL/WS 06-0745, 16 Mar 2006.

14. ABSTRACT

The synthetic conditions for the isolation of the iron-molybdenum nanoc1uster FeMoC, along with its application as a catalyst precursor for VLS growth of SWNTs have been studied. As prepared FeMoC is contaminated with the Keplerate cage without the Keggin template; however, extraction of pure FeMoC may be accomplished by Soxhlet extraction with EtOH. The resulting EtOH solvate is consistent with the replacement of the water ligands coordinated to Fe being substituted by EtOH. FeMoC-EtOH has been characterized by IR, UV-vis spectroscopy, MS, XPS and ^{31}P NMR. The solid state ^{31}P NMR spectrum for FeMoC-EtOH suggests little effect of the paramagnetic Fe^{3+} centers in the Keplerate cage on the Keggin ion's phosphorous. The high chemical shift anisotropy, and calculated T1 and T2 values are consistent with a weak magnetic interaction between the Keggin ion's phosphorus symmetrically located within the Keplerate cage. Increasing the $FeCl_2$ concentration and decreasing the pH of the reaction mixture optimizes the yield of FeMoC. The solubility and stability of FeMoC in H_2O and $MeOH/H_20$ is investigated.

15. SUBJECT TERMS
iron-molybdenum nanoc1uster FeMoC, SWNTs, Keplerate cage, Keggin template, Soxhlet extraction

16. SECURITY CLASSIFICATION OF:			17. LIMITATION OF ABSTRACT:	18. NUMBER OF PAGES	19a. NAME OF RESPONSIBLE PERSON (Monitor)
a. REPORT	b. ABSTRACT	c. THIS PAGE			Benji Maruyma
Unclassified	Unclassified	Unclassified	SAR	58	19b. TELEPHONE NUMBER *(Include Area Code)* N/A

Standard Form 298 (Rev. 8-98)
Prescribed by ANSI Std. Z39-18

Abstract

The synthetic conditions for the isolation of the iron-molybdenum nanocluster FeMoC $[H_xPMo_{12}O_{40} \subset H_4Mo_{72}Fe_{30}(O_2CMe)_{15}O_{254}(H_2O)_{98}]$, along with its application as a catalyst precursor for VLS growth of SWNTs have been studied. As prepared FeMoC is contaminated with the Keplerate cage $[H_4Mo_{72}Fe_{30}(O_2CMe)_{15}O_{254}(H_2O)_{98}]$ without the Keggin $[H_xPMo_{12}O_{40}]^{n-}$ template, however, extraction of pure FeMoC may be accomplished by Soxhlet extraction with EtOH. The resulting EtOH solvate is consistent with the replacement of the water ligands coordinated to Fe being substituted by EtOH. FeMoC-EtOH has been characterized by IR, UV-vis spectroscopy, MS, XPS and ^{31}P NMR. The solid state ^{31}P NMR spectrum for FeMoC-EtOH (δ = -5.3 ppm) suggests little effect of the paramagnetic Fe^{3+} centers in the Keplerate cage on the Keggin ion's phosphorous. The high chemical shift anisotropy, and calculated T_1 (35 ms) and T_2 (8 ms) values are consistent with a weak magnetic interaction between the Keggin ion's phosphorus symmetrically located within the Keplerate cage. Increasing the $FeCl_2$ concentration and decreasing the pH of the reaction mixture optimizes the yield of FeMoC. The solubility and stability of FeMoC in H_2O and MeOH/H_2O is investigated. The TGA of FeMoC-EtOH under air, Ar and H_2 (in combination with XPS) shows that upon thermolysis the resulting Fe:Mo ratio is highly dependent on the reaction atmosphere: thermolysis in air results in significant loss of volatile molybdenum components. Pure FeMoC-EtOH is found to be essentially inactive as a pre-catalyst for the VLS growth of single walled carbon nanotubes (SWNTs) irrespective of the substrate or reaction conditions. However, reaction of FeMoC with pyrazine (pyz) results in the formation of aggregates that are found to be active catalysts for the growth of SWNTs. Activation of FeMoC may also be accomplished by the addition of excess iron. The observation of prior work's reported growth of SWNTs from FeMoC is discussed with respect to these results.

Introduction

The vapor growth of SWNTs from catalyst particles occurs by a general vapor-liquid-solid (VLS) growth mechanism.[1] The growth of SWNTs by VLS is believed to occur via two mechanistic steps: nucleation and growth.[2,3] Nucleation involves both the formation of a catalyst particle and the initial construction of the carbon framework on which the tube is later grown. At growth temperatures (800 – 1000 °C) the catalyst metal atoms aggregate to form a liquid metal nanoparticle. For the growth of SWNTs, it is proposed that the nanoparticle needs to be *ca.* 50 - 200 metal atoms (1 - 100 nm).[4] The size of this particle has been proposed to have an effect on the diameter and type (as defined by the SWNT's m,n value) of tube produced.

The metals most commonly used for SWNT growth are iron, cobalt, nickel, molybdenum, and various bimetallic alloys of these metals.[5] Iron species, such as iron oxides,[6] iron nitrates,[7] $Fe(CO)_5$[8] and ferrocene,[9] have been reported as active catalysts. Irrespective of the iron source, the overall goal has been to form a nanoparticle less than 100 nm. In a recent publication Liu and co-workers[10] have reported the growth of SWNTs using the iron-molybdenum nanocluster $[H_xPMo_{12}O_{40}{\subset}H_4Mo_{72}Fe_{30}(O_2CMe)_{15}O_{254}(H_2O)_{98}]$ (FeMoC) originally reported by Müller and co-workers.[11] The structure of FeMoC (Fig. 1) consists of a tetrahedral reduced Keggin $[H_xPMo_{12}O_{40}]^{3-}$ ion inside a spherical icosahedral giant (Keplerate) cage of the $\{(Mo^{VI})Mo^{VI}_5\}_{12}Fe^{III}_{30}$ type. It was proposed that the individual FeMoC molecules, rather than aggregates, behave as catalyst precursors for the growth of SWNTs. If this is true then this result offers hope of designing particular molecular precursors to SWNT catalysts.

The as-published synthesis of FeMoC has a low yield (4%)[11] and there appears uncertainty as to the color (described as either dark blue or greenish) as well as its solubility and/or stability in water.[10,11] Our initial studies confirmed the variability in the color and analytical purity, prompting a detailed study of the synthesis and the development of appropriate purification procedures. In addition to the purity issue, Liu and co-workers used an iron pre-catalyst in their growth chamber[10] and we were interested to determine if pure FeMoC alone would be a catalyst precursor for the growth of SWNTs or whether the iron pre-catalyst was the

source of the active species. Also, given our ability to purify FeMoC we were interested to determine as to whether individual FeMoC molecules are in-fact a catalyst precursor for the growth of SWNTs. Finally, FeMoC has been shown to undergo a coupling reaction in the solid state at room temperature,[12,13] and it is possible that the aggregation of aged samples is important in the growth of SWNTs.

Results and Discussion

Purification, characterization, and optimization of FeMoC

The reported synthesis of FeMoC involves the addition of $H_3[P(Mo_3O_{10})_4]$ to a pre-made aqueous mixture of $FeCl_2$, Na_2MoO_4, and $MeCO_2H$. The reaction mixture is acidified and allowed to react for 45 min after which time any insolubles are removed by filtration. The filtrate is allowed to evaporate to yield crystals of FeMoC.[11] Following this procedure does indeed yield a dark crystalline material; however, it was found to have inconsistent and irreproducible analysis and spectroscopy suggesting that a mixture of materials co-crystallizes. Furthermore, addition of cold H_2O yields a blue solution and a yellow-green insoluble material. UV-visible spectroscopy of the H_2O soluble blue fraction does not show any of the characteristic nucleus shell charge transfer bands between the host and the Keggin guest (550 nm) associated with the FeMoC structure. Instead it shows a broad band at 723 nm. The ATR spectrum of the blue product does not show any of the peaks associated with FeMoC or the Keplerate cage.[11]

The yellow-green solid is only slightly soluble in H_2O but does give the required band at 550 nm in the UV-visible spectrum, albeit weakly. Investigation of the solubility of the yellow-green solid in a variety of solvents shows that a dark green solution is formed in EtOH with a pale yellow residue remaining. Analysis of each of these fractions indicates that the dark green product formed after washing with cold H_2O and extraction with EtOH is consistent with the spectroscopy associated with the single crystal molecular structure previously reported for FeMoC.**REF**

Based upon XPS, UV-visible, and ATR spectroscopic analysis, the residual yellow solid remaining in the filter appears to be the Keplerate cage without the Keggin template as indicated by the lack of ^{31}P NMR signal. The yellow solid does not dissolve in common solvents, except acidic water. The UV-visible spectrum of a genuine sample of the Keplerate[14] is very similar to the spectrum of the yellow solid from the filter. Similarly, ATR of the Keplerate shows a peak for MoO_t at 960 cm^{-1}; this is observed for yellow residue. The XPS analysis of the yellow residue from the synthesis (Table 1) shows a Fe:Mo:C ratio is 30:69:25 that is similar to an authentic sample of the Keplerate cage (30:72:24). Furthermore, the lack of solubility in water is consistent with previous reports.[14] Thus, based upon the XPS analysis the three fractions from the purification of FeMoC are identified as follows: the blue fraction is a mixture of molybdenum oxides; the green EtOH soluble fraction is FeMoC; the yellow fraction is the Keplerate cage without the Keggin template.

The apparently low solubility of FeMoC, and insolubility of the yellow product (Keplerate cage), allows for the purification of FeMoC by washing the crude product with cold H_2O followed by the Soxhlet extraction of the residue with EtOH. This route produces a saturated solution of FeMoC in EtOH; that may be evaporated to yield a dark green solid. Using the cooled Soxhlet solution after filtration of all solids, the solubility of FeMoC in EtOH as determined (by UV-visible spectroscopy) to be 17.8 $mg.cm^{-3}$ (9.91 x 10^{-4} $mol.dm^{-3}$) at room temperature.

Although spectroscopically identical to the previous reports, the TGA and MS of the green product show the presence of coordinated EtOH. Thus, the green material obtained from Soxhlet extraction has the formula $[H_xPMo_{12}O_{40}\subset H_4Mo_{72}Fe_{30}(O_2CMe)_{15}O_{254}(H_2O)_{98-x}(EtOH)_x]$ where x is calculated to be *ca*. 30. The Maldi-ToF-MS of the Soxhlet product shows a broad peak with the maximum isotope distribution that corresponds closely to a molecular formula of $H_3PMo_{12}O_{40}\subset H_4Mo_{72}Fe_{30}(O_2CMe)_{15}O_{254}(H_2O)_{68}(EtOH)_{30}$ (Calcd. 17977). Based upon this analysis and a consideration of the coordination environments of the H_2O ligands in FeMoC, we propose that EtOH ligands are bound to the Fe^{3+} centers on the outside of the host

cage. Since the exact number of EtOH ligands appears to show a slight dependence on the length of the Soxhlet extraction process (i.e., the time and/or concentration of the refluxing EtOH solution) we designate the EtOH complexed product as FeMoC-EtOH.

The AFM of FeMoC-EtOH spin-coated onto mica shows individual nanoparticles with a height of 2 nm. The theoretical diameter of FeMoC (based upon the X-ray crystal structure) is 2.1 nm. Thus, within experimental error the diameter observed is consistent with the retention of the FeMoC structure in FeMoC-EtOH. The UV-visible spectrum of purified FeMoC-EtOH (Fig. 2) shows bands reported previously to be characteristic of an intervalence [Mo(V) $\rightarrow$Mo(VI)] charge transfer in the Keggin cluster (880 and 1045 nm) and the nucleus shell charge transfer between the host and the Keggin guest (550 nm).

The XPS analysis of FeMoC-EtOH (Table 2) shows a Fe:Mo ratio (1:2.7) consistent with the formulation of the encapsulated molybdate ion in the supramolecular cage (calculated = 1:2.8). The calculated concentration of phosphorus is slightly high, however, the low intensity of the P 2p peak (and hence the poor signal to noise) makes quantification difficult. There are signals within the C1s and O1s that correspond to the C-O portion of the acetates (Fig. 3) with an O:C ratio of *ca*. 1.5 (as compared to the theoretical value of 2.0). Furthermore, the carbon content is consistent with the substitution of coordinated water for EtOH ligands.

Müller and co-workers have previously reported[11] that FeMoC is a highly paramagnetic cluster containing 150 unpaired electrons associated with 30 octahedral high-spin d^5 Fe^{3+} centers. Our ability to prepare purified samples of FeMoC (albeit with EtOH associated with the Fe^{3+} centers instead of H_2O) prompted an investigation of the ^{31}P NMR spectrum of FeMoC-EtOH since the shift and relaxation of the ^{31}P nucleus can be uniquely influenced by the 30 paramagnetic centers positioned in a spherical manner at a distance of *ca*. 10 Å. The solid state ^{31}P NMR spectrum for FeMoC-EtOH is shown in Fig. 4 along with the spectrum of $H_3[P(Mo_3O_{10})_4]$ for comparison. The spectrum of $H_3[P(Mo_3O_{10})_4]$ (Fig. 4a) shows a single resonance at δ = –4.2 ppm typical of PO_4 coordination environment.[15] The chemical shift for FeMoC-EtOH (δ = -5.3 ppm) is close to that of $H_3[P(Mo_3O_{10})_4]$ suggesting little effect of the

paramagnetic Fe^{3+} centers in the Keplerate cage on the Keggin ion's phosphorous. However, we note that the spectrum for FeMoC-EtOH (Fig. 4b) shows a higher chemical shift anisotropy (the asymmetry parameter is near 1 indicating an extremely symmetric environment), which suggests that the Keggin ion is located centrally within the Keplerate cage. Fig. 5 shows a pseudo 2D inversion recovery data set resulting from the application of the 180-τ-90-acquire sequence. From this data we obtain the plot in Fig. 6, that is the intensity of the center band versus τ, and subsequently the T_1 (35 ms). Phosphates generally have T_1 in the range of 0.1 – 10 seconds.[16] We propose the major contribution to the shorter T_1 in FeMoC-EtOH is the paramagnetism of the Fe^{3+} centers in the Keplerate cage. But the fact that we can see one at all suggests that their influence is not overwhelming. The T_2 for FeMoC-EtOH is obtained from a pseudo 2D CPMG data set (T_2 isolation by spin echo), shown in Fig. 7 and 8. The calculated T_2 (8 ms) is within the normal range for phosphates in the solid state.[17] The solid state ^{31}P NMR data is consistent with a weak interaction between the central phosphorus and the surrounding Keplerate cage.

A consideration of the stoichiometry of the reaction as reported in the literature (Table 3) shows that both $FeCl_2$ and Na_2MoO_4 are limiting reagents, while the $MeCO_2H$ is in large excess. Performing the reaction under stoichiometric conditions results in only a small increase in the isolated yield. Despite the Na_2MoO_4 being a limiting reagent, increasing its concentration resulted in the reduction in the yield of FeMoC. A similar effect was observed by the reduction of $MeCO_2H$ (Table 3). Conversely, an increase in the $FeCl_2$ content resulted in a dramatic increase in FeMoC yield to *ca*. 12%. Further increases resulted in higher yields. The oxidation state of the iron reagent is clearly important since substituting Fe(III) for Fe(II) resulted in no FeMoC being formed, despite the presence of Fe(III) in FeMoC's Keplerate cage. A batch of FeMoC was prepared by changing the order of the reaction steps by putting the Keggin ion ($H_3[P(Mo_3O_{10})_4]$) in first. The UV spectrum was unchanged, and no improvement in yield was achieved.

As discussed above, the literature synthesis of FeMoC suggested the pH should be adjusted to 2 prior to evaporation of the solution. To determine if the pH of the solution affects

FeMoC formation, a single batch of FeMoC was prepared, divided into four equal parts and the pH adjusted (Fig. 9). Above pH 2.75, FeMoC is not formed; as the pH of the solution is lowered the yield of FeMoC is increased. The pH of the reaction also appears to have some effect on the rate of the reaction; at lower pH the precipitation is initiated more rapidly. Given that the pK_a values for $H_3[P(Mo_3O_{10})_4]$ are 1.61 ±0.10, 2.28 ±0.08, 2.41 ±0.12,[18] it appears that the highest yield of FeMoC is obtained under conditions where the $H_3[P(Mo_3O_{10})_4]$ is protonated.

Investigating the solubility/reactivity of FeMoC with other common solvents showed that stable solutions were formed with EtOH, MeOH and H_2O. Suspensions (without apparent reaction) were observed for MeCN, acetone, Et_2O, IPA, CH_2Cl_2, $CHCl_3$, pentane, hexane, benzene and toluene. In toluene a colloidal suspension appears to be stable for 24 hours, however, precipitation occurs after that time. Suspensions in THF and DMF changed color to yellow and orange, respectively, indicating chemical reaction (possibly ligand substitution), but no solubility was observed. The formation of a yellow (iron containing) product was also observed for the long-term storage of FeMoC in MeOH solution. The solubility of FeMoC in MeOH (2 $mg.mL^{-1}$ @ 25 °C) is poor compared to that in EtOH (12 $mg.mL^{-1}$ @ 25 °C), and over the 30-day period some of the FeMoC precipitated out of solution, but the solubility is still adequate for our needs. In contrast, FeMoC is indefinitely stable in EtOH solution, and no change is observed in the UV-visible spectrum of an EtOH solution after 4 weeks.

Liu and co-workers have reported that FeMoC was soluble in water;[10] however, in their original report Müller *et al*. suggested it was insoluble.[11] Given this confusion and the reported blue color of the former product, we have investigated the stability of purified FeMoC(EtOH) in water. FeMoC was dissolved in water (0.5 $mg.mL^{-1}$) and the pH adjusted to appropriate values with HCl. At pH 1 FeMoC is only partially soluble, and after 24 h no peaks indicative of FeMoC are observed in the UV-visible spectrum. As may be seen from Fig. 10, the stability of FeMoC increases with increased pH. At pH 2 FeMoC is essentially decomposed after 2 days; however, at pH 3 - 5 FeMoC bands in the UV-visible spectra were discernable through 7 days. Along with the decomposition of FeMoC there is a concomitant decrease in the pH of the solutions after 9

days from 4 to 3.6 and from 5 to 4.2. The desire to react FeMoC with functionalized SWNTs in a water solution, but the low stability of FeMoC in water, prompted the investigation of its stability in MeOH/H_2O mixtures. As may be seen from Fig. 11, FeMoC is completely stable in MeOH solution over 9 days at room temperature. During that corresponding time decomposition of over 80% occurs; however, use of a 1:1 MeOH/H_2O solution results in the retention of 90% after 9 days.

Thermal decomposition of FeMoC-EtOH

Liu and co-workers reported[11] that as a catalyst precursor for the growth of SWNTs, FeMoC was heated to 700 °C in air (to decompose the organic ligands) and then reduced in H_2 at 900 °C prior to introduction of the growth gas. In our growth studies we have found that the efficacy of FeMoC as a catalyst precursor is dependant on the protocol for conversion to a metal catalyst. In order to understand these results we have investigated the thermal decomposition of purified FeMoC-EtOH by TGA, TGA-MS, and XPS.

The TGA of samples of FeMoC-EtOH heated to 1000 °C are shown in Fig. 12; the Fe:Mo ratio of the products formed upon heating to 400, 700 and 900 °C are given in Table 4. TGA-MS shows that, irrespective of the atmosphere, the mass loss that occurs prior to 200 °C is due to loss of coordinated EtOH and H_2O, while the mass loss at *ca*. 400 °C is consistent with the decomposition of the organic substituents and loss of additional H_2O (presumably the water of coordination that is inside the FeMoC cage).

Under H_2 atmosphere there is a further mass loss at *ca*. 600 °C that is consistent with the reduction of the metal oxide (formed upon pyrolysis) to metal (mass loss: calcd. 67%; exp. 72%). This is confirmed by XPS analysis (Table 4) that shows only a small change in the Fe:Mo ratio. As expected there is no reduction reaction in either air or argon at 600 °C, though both show mass loss at higher temperatures (Fig. 12). Based upon XPS analysis the continuing mass loss starting at 800 °C in air is consistent with the sublimation of molybdenum oxides. Under argon the Fe:Mo ratio appears to change but towards a slight loss of iron (Table 4). However, the

mass loss starts at a lower temperature but is incomplete. We propose that under an oxidizing environment (such as air) all the molybdenum is converted to volatile oxides, while under argon the oxide material formed upon pyrolysis contains a mixture of molybdenum oxides (or a mixed iron-molybdenum oxide) of which only a fraction are volatile below 1000 °C. Based upon the forgoing, we propose that the choice of thermal treatment prior to reduction with H_2 and introduction of the SWNT growth gas (e.g., CH_4, C_2H_4, etc.) will control the Fe:Mo ratio.

VLS growth of SWNTs from FeMoC

The use of FeMoC as a suitable catalyst precursor for the growth of SWNTs is based on the rationale that it is a discrete cluster, which when reduced should form a 1–2 nm iron/molybdenum particle. However, as noted in the Introduction, the first demonstration of its use as a catalyst precursor not only required an iron-containing pre-catalyst for successful growth, but also described the FeMoC as being dark-blue[10] in color (whereas the original report of its synthesis described its color as green).[11] Given our isolation of pure FeMoC-EtOH, we have investigated its use as a catalyst precursor in the VLS growth of SWNTs on both Si and spin-on-glass (SOG) substrates in the absence of any pre-catalysts.

In contrast to other molecular- or nanoparticle-derived catalyst precursors under identical growth conditions,[19] growth of SWNTs from FeMoC-EtOH on Si and SOG substrates was not observed when using either C_2H_4 at 750 °C or CH_4 at 800 °C as the growth gas (irrespective of the reduction protocols used to activate the precursor). It is possible, however, to get sparse growth of SWNTs (ca. 1-2 SWNTs per 1000 μm^2 area) by using CH_4 at 900 °C (see Experimental). As may be seen from the AFM image in Fig. 13, essentially no SWNTs are grown during a 15 min period, despite the presence of a significant surface coverage of isolated catalyst precursor particles (*ca*. 200 particles per 1 μm^2 area). The single short (*ca*. 300 nm) SWNT observed in Fig. 13 was found only after extensive searching over a 2000 μm^2 area. Multiple reaction runs under identical conditions yielded similarly poor results. There appears to be no reproducible substrate dependence on growth; however, RCA-cleaned Si substrates appear

to nucleate more amorphous carbon deposits during growth runs in comparison to RCA-cleaned SOG substrates which results in dirtier samples that are more difficult to image by AFM.

These experiments were repeated in two different growth chambers (at Rice University and at Wright Patterson AFB), and the recurring result is that essentially no growth is seen for pure, freshly prepared FeMoC-EtOH deposited onto either Si or SOG substrates. In addition, we have performed growth runs in which samples of the catalyst precursor $[Fe_3O(O_2CMe)_6(EtOH)_3]$ on either Si or SOG were placed side-by-side with those prepared from pure FeMoC-EtOH.[19] In these experiments, the FeMoC samples showed virtually no growth, while the $[Fe_3O(O_2CMe)_6(EtOH)_3]$ samples exhibited significant growth (*ca*. 2-4 SWNTs per 25 μm^2 area). Thus, we have shown that FeMoC, itself, is an extremely poor catalyst precursor for the growth of SWNTs. This result questions prior research reporting the growth of SWNTs from FeMoC. There are two possible reasons that SWNTs were previously observed. First, both the iron-containing pre-catalyst and impurities remaining in the green FeMoC used in the prior work[10] could be responsible for the "activation" of FeMoC to a state where it becomes a decent catalyst precursor. Second, FeMoC has been shown to undergo a coupling reaction in the solid state at room temperature,[11] and it is possible that the aggregation of precursor particles affects SWNT growth. In order to simulate both of these effects, we have investigated the forced aggregation of FeMoC using the bridging pyrazine (pyz) ligand. Nitrogen donor ligands (such as pyrazine and pyridine) readily replace the coordinated EtOH molecules.[20]

Spin coating SOG-coated wafers with solutions formed from the reaction of EtOH solutions of FeMoC and pyz results in the formation of aggregates (FeMoC-pyz), presumably by the pyz acting as a bridging ligand between FeMoC molecules.[21] Reduction with H_2 under conditions used for the growth of SWNTs (900 °C, 225 sccm, 15 min) resulted in their reduction. AFM characterization shows that the size of the aggregate is dependent on the FeMoC:pyz ratio in solution (Fig. 14). Thus, the reaction of FeMoC with pyz allows for the controlled formation of aggregates and the simulation of the solid state Fe-O-Fe coupling process that occurs during the aging of FeMoC.[11] AFM particle analysis of H_2-reduced pure FeMoC-EtOH on SOG

revealed a surface covered with a wide distribution of aggregates possessing diameters ranging from 2–20 nm. In contrast, analogous analysis of the 1:25 FeMoC-pyz solution on SOG showed that the surface was covered with a narrow distribution of aggregates possessing an average diameter of 4 nm. Both of these reduced samples were placed side-by-side in the growth chamber to evaluate the suitability of the controlled aggregates as catalyst precursors for the VLS growth of SWNTs. After being heated to the growth temperature (900 ˚C) under argon, the samples were re-reduced with H_2 (225 sccm, 5 min) to remove any oxide layers formed during the AFM characterization; after the 5 min, CH_4 (225 sccm) was introduced while leaving the H_2 on (to reduce amorphous carbon formation) and allowed to flow for a growth period of 15 min.

Use of the 1:25 FeMoC-pyz aggregates as catalyst precursors results in a significant increase (~500x) in the yield of SWNTs grown on SOG (15-25 SWNTs per 25 μm^2 area) as compared to pure FeMoC-EtOH on SOG, which also exhibited pitiful growth (1-2 SWNTs per 1000 μm^2 area) under these new growth conditions. In addition, the average length is increased while the average diameter is narrow (Table 5) as may be seen from the AFM image in Fig. 15. While the overall SWNT yield per reduced precursor particle (~1%) is still lower than observed for other molecular precursors, it is still a significant improvement over pure FeMoC (<0.05%). In fact, SWNTs are easily observed across entire wafers for samples prepared from 1:25 FeMoC-pyz aggregates, in sharp contrast to the results for FeMoC alone. Thus it appears that the formation of a narrower distribution of small aggregates promotes the “activity” of FeMoC toward catalysis. The Raman spectrum of SWNTs grown from FeMoC-EtOH solutions shows the characteristic G-band at 1590 cm^{-1}, confirming the formation of SWNTs as opposed to multi-walled carbon nanotubes.

In order to simulate the presence of either an iron-containing pre-catalyst or impurities in FeMoC, we have reacted the 1:25 FeMoC-pyz aggregate with $Fe(NO_3)_3$. The AFM particle analysis indicates that the 1:25 FeMoC-pyz aggregates have an average diameter of 4 nm; however, given the excess of pyz ligands plausibly present at the surface of the aggregates, there should be additional coordination sites available for the Fe^{3+}. Reaction of FeMoC, pyz, and

$Fe(NO_3)_3$ in a 1:25:25 ratio results in the formation of a narrow distribution of aggregates on SOG possessing an average diameter of 11 nm upon reduction with H_2 (Fig. 14d). The 1:25:25 FeMoC-pyz-$Fe(NO_3)_3$ on SOG sample was compared to pure FeMoC-EtOH on SOG in a VLS growth run using the identical procedure used for the aforementioned 1:25 FeMoC-pyz comparison. The 1:25:25 FeMoC-pyz-$Fe(NO_3)_3$ on SOG sample also exhibited significantly more growth (15-25 SWNTs per 25 μm^2 area, Fig. 16) than the reliably poor FeMoC-EtOH on SOG sample (1-2 SWNTs per 1000 μm^2 area). Furthermore, relatively higher yields of long SWNTs were grown per precursor particle (~2%, Table 5). This result suggests that the presence of the iron-containing pre-catalyst or iron impurities could explain the previously reported catalytic activity for FeMoC.

Conclusions

We have reported the optimized synthesis of FeMoC with respect to yield and purification. Purification is enabled via ligand exchange (H_2O with EtOH), while increasing the $FeCl_2$ concentration and lowering the reaction pH below the value previously reported resulted in an increase in the yield. In contrast to previous work,[10] purified FeMoC is a poor catalyst precursor for the VLS growth of SWNTs. However, FeMoC may be activated by the controlled formation of small aggregates (d = 4 nm) using the bridging ligand pyrazine. Alternatively, the addition of additional iron also appears to activate the FeMoC. These results suggest that a small degree of molecular aggregation is important to achieve the critical size necessary for FeMo catalysis (i.e., an individual FeMoC molecule may not contain sufficient metal atoms (114) to make an active catalyst). However, when the aggregates become too large (>10 nm), they may become more susceptible to side reactions that inactivate the catalysts to VLS growth of SWNTs, such as silicide formation with the substrate surface or nucleation of the growth gas to form amorphous carbon shells. Nevertheless, the presence of additional iron in larger aggregates (d = 11 nm) appears to overcome these barriers to promote the VLS growth of SWNTs. Taken together, these results have significant implications regarding the required size of a catalyst particle for the VLS

growth of SWNTs. Our studies in this area are continuing. The ability to purify FeMoC through ligand exchange offers a route to functionalization of this interesting magnetic nanoparticle for growth of self assembled monolayers and 2D arrays.

Experimental

Solvents were purchased from Fisher Scientific and used as received. $FeCl_2$, Na_2MoO_4, and $HPMo_{12}O_{40}$ were obtained from commercial vendors (Sigma-Aldrich) and stored in a desiccator prior to use. All organic reagents (Aldrich, TCI America, Alfa Aesar) solvents (Fisher Scientific) were used as received. Keplerate synthesis was accomplished using a modification of the literature method.[22]

Thermogravimetric analyses were performed on a Seiko TG/DTA 200 using Ar or air as the carrier gas. Thermogravimetric/mass spectrometry analyses were performed on a Seiko TG/DTA 200 using H_2 and air as the carrier gases. IR spectra (4000 – 400 cm^{-1}) were recorded on a Nicolet 760 FT-IR spectrometer, and analyzed using a diamond cell ATR and using a 50x long working objective lens. The UV absorption measurements were carried out using a Cary 910 UV/Vis Spectrophotometer.

Solid state ^{31}P CPMAS NMR spectra were measured on a Bruker Avance 200 spectrometer at 81 MHz. Samples were measured using a 7 mm extended VT MAS probe with 7 mm long-barrel ZrO_2 rotors and plugs and Kel-F fluoropolymer caps. Chemical shifts were referred to the $NH_4[H_2PO_4]$ (δ = 0.8 ppm) by sample replacement. All the spectra were collected with high power ^1H decoupling. Spectra were acquired using a 90° pulse of 3.5 μs and a spectral width of 149,253 Hz. Bloch decay spectra were collected at a spinning speed of 6.00 kHz for 20480 scans with power-gated high-power ^1H decoupling over a spectral width of 150 kHz. Measurement conditions for FeMoC as follows: spinning frequency, 6 kHz; pulse repetition time, 150 ms; number of points, 4,462 (1D), 14,910 (T_1 IR), 2,970 (T_2 CPMG); number of scans, 20k. Measurement conditions for $H_3[P(Mo_3O_{10})_4]$ as follows: spinning frequency, 6 kHz; pulse repetition time, 30 s; number of points, 14,910; number of scans, 1992. T_1 relaxation times were

measured via the standard inversion recovery method with power-gated high-power ^1H decoupling where appropriate for 8000 scans. Values of τ were selected initially by a telescoping series of values ranging from 1 ms to 1 s. T_2 relaxation times were measured via the Carr-Purcell-Meiboom-Gill (CPMG) spin-echo decay method with power-gated high-power ^1H decoupling and an echo decay time 2τ of 1 ms per echo iteration for 8000 scans.

A Physical Electronics (PHI 5700) XPS/ESCA system with base pressure of 5×10^{-9} Torr was used to record X-ray photoelectron spectra. A monochromatic Al-X_α source at 350 W was used with an analytical spot size of 1.2 mm and 60° takeoff angle. Atomic concentration values were calculated with PHI Multipak software using factory-calibrated values for the sensitivity factors of the respective elements. Binding energy values were referenced externally to an Au 4f peak at 84.00 eV, and internally to a C 1s binding energy of 284.50 eV (NIST XPS database). The speciation and composition variation was obtained by recording the multiplex spectra for C 1s, O1s, P 2p, Fe2p and Mo 3d elemental energy levels. Samples were ground lightly onto indium foil so that they would make a thin, still-crystalline film.

AFM measurements were taken on a Digital Instruments NanoScope IIIa scanning probe microscope in tapping mode. A RTESP type Nanoprobe™ SPM Tip with a drive frequency of 300 kHz was used. Images were taken at a scan frequency of 1-2 Hz and 256-512 samples/line. Samples were prepared by taking an aliquot of the cluster solution diluted to a final concentration of 0.1 μM in EtOH. One drop of the solution was spin coated onto a freshly prepared mica surface. The sample was spun for 5 min. to ensure that all of the EtOH had evaporated.

Synthesis of FeMoC-EtOH.

The baseline synthesis of FeMoC was carried out by a modification of the literature reported method.[11] $FeCl_2.4H_2O$ (1.00 g, 5.03 mmol) is dissolved in Millipore water (75 mL) resulting in a clear slightly yellow solution. To this solution $Na_2MoO_4.2H_2O$ (2.00 g, 8.27 mmol) was added, turning the solution a cloudy rust-red. Glacial acetic acid (10 mL, 59 mmol)

was added turning the solution from cloudy to clear red; followed by $H_3[P(Mo_3O_{10})_4]$ (2.50 g, 1.37 mmol) producing a dark blue solution. The solution's pH was adjusted to 2 with HCl and then stirred at room temperature for 45 minutes. The solution was then filtered through a fine glass frit. The filtrate was kept in an open beaker for at least 5 days to allow crystallization. The crystals were then vacuum filtered, washed with H_2O and dried. The solid was transferred to a filter thimble and placed inside a Soxhlet extractor. EtOH was refluxed in the extractor overnight and a dark green solution was collected. Yield: 0.083 g, 4.03%. Variations on the stoichiometry of reaction were carried out according to the reagent ratios given in Table 3. Solubility of FeMoC in EtOH Soxhlet mother liquor: 17.8 $mg.mL^{-1}$. Solubility of pre-formed FeMoC dissolved in EtOH at RT: 12 $mg.mL^{-1}$. XPS Analysis (eV): 726.1 (Fe $2p^{1/2}$), 712.0 (Fe $2p^{3/2}$), 532.8 (O 1s, $\underline{O}_2CMe$), 530.1 (O 1s, MO_x), 288.8 (C 1s, $O_2\underline{C}Me$), 284.5 (C 1s, $\underline{C}H_3$ and $\underline{C}_2H_6$), 236.0 (Mo $3d^{3/2}$), 232.8 (Mo $3d^{5/2}$), 133.5 (P 2p).

Preparation of FeMoC-pyz aggregates.

Stock solution of FeMoC (25 μM) and pyrazine (2.5 mM) in EtOH were prepared. From the pyrazine solution a 20 mL aliquot was removed and diluted with EtOH to a volume of 200 mL to yield a 0.25 mM solution. The respective volumes of the stock solutions were transferred to a 50-mL Schlenk flask fitted with a condenser and a magnetic stir bar. EtOH was added to dilute the mixture to a total volume of 25 mL (Table 6). The flask was externally heated to reflux under an inert N_2 atmosphere and allowed to stir for 1.5 hours. Two drops of the solutions were then spin coated onto an appropriate wafer for AFM analysis and VLS growth. The addition of $Fe(NO_3)_3{\cdot}9H_2O$ (0.0025 g, 6.2 mmol) dissolved in EtOH (2.5 mL) to the FeMoC-pyz aggregate (1:25) resulted in an iron rich aggregate. The size of the reduced aggregates was determined by spin coating (3,000 rpm for 40 s) solutions of the aggregates onto SOG coated Si wafers. The aggregates were subsequently placed in the VLS growth chamber (see below). The reactor was flushed with Ar (1000 sccm) as the temperature was raised to 900 °C at 10 $°C{\cdot}min^{-1}$. Once at

temperature the H_2 (225 sccm) was turned on followed by the Ar being turned off. The reduction with H_2 lasted for 15 min., after which the Ar was turned back on and the H_2 flow ceased.

VLS Growth of SWNTs from FeMoC and FeMoC-pyz aggregates.

Either a Thermolyne 211000 or Lindberg Blue Minimite tube furnace with a mullite tube and plumbed with UHP gases was used for the growth runs. Flow rates were 150-1000 sccm for argon and 225 sccm for both CH_4 and H_2. Substrates were of either n-type silicon or n-type silicon coated with spin-on-glass (SOG). An n-type 100 silicon wafer was coated with a 100 nm layer of spin-on-glass (Accuglass® T111) and was cured at in air 700 °C for 1 h, and then cut into 1 cm^2 pieces. By varying spin speed, it is possible to obtain thickness from 86 – 360 nm. A second n-type silicon wafer was submerged in a solution of 30% H_2O_2 (10 mL), 28% NH_4OH (10 mL), and deionized H_2O (50 mL) and allowed to sit for 10 minutes to remove any native oxide layers. The wafers were then removed from the solution and rinsed with deionized H_2O followed by EtOH and the placed into an oven at 150 °C for 10 minutes to dry. Two drops of the appropriate FeMoC or FeMoC-pyz aggregate solutions were then spin coated onto the wafer at 3,000 rpm for 40 sec. The silicon wafer were placed in either a ceramic or quartz boat and positioned within the hot zone of the tube furnace. The tube was flushed with argon as the temperature was raised to 900 °C at 10-20 $°C.min^{-1}$. Once at temperature the H_2 was turned on followed by the Ar being turned off. The reduction with H_2 lasted for 15 min. immediately followed by turning on CH_4 growth gas. The growth run lasted for 15 min., after which the Ar was turned back on and the H_2 and CH_4 were turned off. The tube was allowed to cool to room temperature. With these flow rates and temperatures the formation of amorphous carbon was not observed.

Acknowledgements.

Financial support for this work is provided by the Robert A. Welch Foundation and the Defense Advanced Research Projects Agency (DARPA).

References

1 E. F. Kukovitsky, S. G. L'vov, and N. A. Sainov, *Chem. Phys. Lett.*, 2000, **317**, 65.

2 J. Gavillet, A. Loiseau, F. Ducastelle, S. Thair, P. Bernier, O. Stéphan, J. Thibault, and J. –C., Charlier, *Carbon*, 2002, **40**, 1649.

3 A. Gorbunov, O. Jost, W. Pompe, and A. Graff, *Carbon*, 2002, **40**, 113.

4 F. Ding, A. Rosén, and K. Bolton, *J. Chem. Phys.*, 2004, **121**, 2775.

5 F. Banhart, N. Grobert, M. Terrones, J. –C. Charlier, and P. M. Ajayan, *Int. J. Mod. Phys. B*, 2001, **15**, 4037.

6 H. Ago, K. Nakamura, N. Uehara, and M. Tsuji, *J. Phys. Chem. B*, 2004, **108**, 18908.

7 S. C. Lyu, B. C. Liu, S. H. Lee, C. Y. Park, H. K. Kang, C. W. Yang, and C. J. Lee, *J. Phys. Chem. B*, 2004, **108**, 1613.

8 P. Nikolaev, M. J. Bronikowski, R. K. Bradley, F. Rohmund, D. T. Colbert, K. A. Smith, and R. E. Smalley, *Chem. Phys. Lett.*, 1999, **313**, 91.

9 H. M. Cheng, F. Li, G. Su, H. Y. Pan, L. L. He, X. Sun, and M. S. Dresselhaus, *Appl. Phys. Lett.*, 1998, **72**, 3282.

10 L. An, J. M. Owens, L. E. McNeil, and J. Liu, *J. Am. Chem. Soc*., 2002, **124**, 13688.

11 A. Müller, S. K. Das, P. Kögerler, H. Bögge, M. Schmidtmann, A. X. Trautwein, V. Schünemann, E. Krickemeyer, and W. Preetz, *Angew. Chem. Int. Ed*., 2000, **39**, 3414.

12 A. Müller, E. Krickemeyer, S. K. Das, P. Kögerler, S. Sarkar, H. Bögge, M. Schmidtmann, and S. Sarkar, *Angew. Chem. Int. Ed*., 2000, **39**, 1612.

13 A. Müller, S. K. Das, M. O. Talismanova, H. Bögge, P. Kögerler, , M. Schmidtmann, S. S. Talismanov, M. Luban, and E. Krickemeyer, *Angew. Chem. Int. Ed.*, 2002, **41**, 579.

14 A. Müller, S. Sakar, S. Q. N. Shah, H. Bögge, M. Schmidtmann, S. Sakar, P. Kögerler, B. Hauptfleisch, A. X. Trautwein, and V. Schünemann, *Angew. Chem. Int. Ed*., 1999, **38**, 3238.

15 B. C. Tischendorf, D. J. Harris, J. U. Otaigbe, and T. M. Alam, *Chem. Mater*., 2002, **14**, 341; M. Witschas and H. Eckert, *J. Phys. Chem. A*, 1999, **103**, 10764; L. B. Moran, J. K. Berkpwitz, and J. P. Yesinowski, *Phys. Rev. B*, 1992, **45**, 5347.

16 W. T. Beaudry, G. W. Wagner, and J. R. Ward, *J. Mol. Catal*., 1994, **93**, 221.

17 C. Mercier, L. Montagne, H. Sfihi, G. Palavit, J. C. Boivin, and A. P. Legrand, *J. Non-Cryst. Solids*, 1998, **224**, 163.

18 (a) F. Ding, K. Bolton, and A. Rosén, *J. Phys. Chem. B*, 2004, **108**, 17369. (b) K. Seo, C. Kim, B. Kim, Y. H. Lee, and K. Song**,** *J. Phys. Chem. B*, 2004, **108**, 4308.

19 D. Ogrin, R. Colorado, Jr., B. Maruyama, M. J. Pender, R. E. Smalley, and A. R. Barron, *Dalton Trans*., 2006, in press.

20 R. Colorado, Jr., D. Ogrin, and A. R. Barron, submitted for publication.

21 D. Ogrin, L. H. van Poppel, S. G. Bott and A. R. Barron, *Dalton Trans*., 2004, 3689.

22 (a) A. Müller, S. Sarkar, S. Q. N. Shah, H. Bögge, M. Schmidtmann, S. Sarkar, Paul Kögerler, B. Hauptfleisch, A. X. Trautwein, and V. Schünemann, *Angew. Chem. Int. Ed.*, 1999, **38**, 3238. (b) A. Müller, E. Krickemeyer, H. Bögge, M. Schmidtmann, and F. Peters**,** *Angew. Chem. Int. Ed.*, 1998, **37**, 3360.

Table 1. XPS elemental ratio analysis for the yellow byproducts from FeMoC synthesis.

Elemental Ratio	Fe	Mo	O	C
Yellow residue (Exp.)	30	68.5	222	24.6
Keplerate (Calcd.)	30	72	382	24

Table 2. XPS elemental ratio analysis for the products from FeMoC synthesis.

Elemental Ratio	Fe	Mo	P	O	C
FeMoC (Calcd.)	30	84	1	422	30
FeMoC-EtOH (Exp.)	30	79.5	<3[a]	316	68.0
$FeMoC(EtOH)_{30}$ (Calcd.)	30	84	1	422	60
Yellow residue (Exp.)	30	68.5	0	222	24.6
Keplerate (Calcd.)	30	72	0	382	24

[a] Exact atomic ratio difficult to determine due to low signal to noise.

Table 3. Product yield as a function of reagent ratio.[a]

Experiment	Na_2MoO_4 (mmol)	$FeCl_2$ (mmol)	$MeCO_2H$ (mmol)	$H_3[P(Mo_3O_{10})_4]$ (mmol)	Yield (%)[b]	Notes
1	8.27	5.03	174	1.37	4.0	Literature
2	72	30	15	1	4.7	Stoichiometric
3	8.27	5.03	87	1.37	3.4	$[MeCO_2H]/2$
4	16	5.03	174	1.37	1.7	$2[Na_2MoO_4]$
5	8.27	5.03 ($FeCl_3$)	174	1.37	0	Fe^{3+} versus Fe^{2+}
6	8.27	10	174	1.37	12.4	$2[FeCl_2]$
7	8.27	20	174	1.37	25.3	$4[FeCl_2]$

[a] All reactions normalized to pH = 2 and stirred for 45 minutes prior to filtration.

[b] Based upon Na_2MoO_4 as the limiting reagent.

Table 4. Fe:Mo ratio as determined by XPS for FeMoC-EtOH thermal decomposition products under air, argon, and hydrogen atmospheres.[a]

Carrier gas	Temperature (°C)		
	400	700	900
air	1:2.61	1:2.72	1:0.47
Ar	1:2.58	1:2.61	1:2.94
H_2	1:2.53	1:2.36	1:2.32

[a] Measured Fe:Mo ratio prior to thermolysis = 1:2.65.

Table 5. Comparison of lengths and diameters for SWNTs.

Growth method	Substrate	Average length (μm)[a]	Average diameter (nm)	Ref
FeMoC	Si	> 1	1.3 (±0.50)	c
FeMoC-EtOH	Si	>2[b]	1.1 (±0.1)	d
FeMoC-EtOH	SOG	0.3[b]	2.1 (±0.1)	d
FeMoC-pyz (1:25)	SOG	> 1[b]	1.25 (±0.25)	d
FeMoC-pyz-$Fe(NO_3)_3$ (1:25:25)	SOG	> 1[b]	1.6 (±0.2)	d

[a] The length of the as grown SWNT will depend on the reaction time.

[b] Reaction time 15 min.

[c] L. An, J. M. Owens, L. E. McNeil, and J. Liu, *J. Am. Chem. Soc*., 2002, **124**, 13688.

[d] This work.

Table 6. FeMoC:pyz aggregate formation.

FeMoC solution (mL)	Pyz solution (mL)	EtOH (mL)	FeMoC:pyrazine molar ratio
10	0.100	14.9	10:1
10	0.200	14.8	5:1
10	1	14	1:1
10	5	10	1:5
10	10	5	1:10
10	12.5	2.5	1:25

[a] 25 μM in EtOH. [b] 0.25 mM in EtOH.

Legends for Figures.

Fig. 1. Computer representation of FeMoC based upon single crystal data showing the 'cluster-within-a-cage' structure. The central Keggin ion is shown in green, the molybdenum atoms of the Keplerate cage are shown in blue, iron atoms are in yellow and oxygen atoms in red.

Fig. 2. UV-visible spectra of FeMoC-EtOH in EtOH.

Fig. 3. X-ray photoelectron spectra of (a) C 1s and (b) O 1s for FeMoC-EtOH.

Fig. 4. ^{31}P NMR spectra of (a) FeMoC-EtOH and (b) $H_3[P(Mo_3O_{10})_4]$.

Fig. 5. Pseudo 2D inversion recovery data set for ^{31}P NMR of FeMoC-EtOH.

Fig. 6. The height of the center band (δ = -5.5 ppm) for the ^{31}P NMR spectrum of FeMoC-EtOH versus τ (T_1 = 35 ms).

Fig. 7. Pseudo 2D cpmg data set (T_2 isolation by spin echo) for FeMoC-EtOH.

Fig. 8. The height of the center band (δ = -5.5 ppm) for the ^{31}P NMR spectrum of FeMoC-EtOH versus τ (T_2 = 8 ms).

Fig. 9. Plot of FeMoC-EtOH yield as a function of reaction pH.

Fig. 10. Plot of concentration versus time for FeMoC in aqueous solution at pH 2 (■), 3 (▫), 4 (●) and 5 (○).

Fig. 11. Plot of concentration versus time of FeMoC in MeOH (▫), MeOH/H_2O 1:1 (●), and H_2O at pH 4.5 (■) at room temperature.

Fig. 12. TGA of FeMoC-EtOH under different atmospheres.

Fig. 13. AFM image of single SWNT from VLS growth of pure FeMoC-EtOH. Image is 2 μm x 2 μm.

Fig. 14. AFM images of (a) FeMoC, FeMoC:pyz aggregates [(b) 1:1 and (c) 1:25] and (d) FeMoC:pyz:$Fe(NO_3)_3$ (1:25:25) after 15 minute H_2 reduction at 900 °C. All images are 1 μm x 1 μm.

Fig. 15. AFM image of VLS grown SWNTs from FeMoC:pyz (1:25). Image is 2 μm x 2 μm.

Fig. 16. AFM image of VLS grown SWNTs from FeMoC:pyz:$Fe(NO_3)_3$ (1:25:25). Image is 5 μm x 5 μm.

Fig. 1.

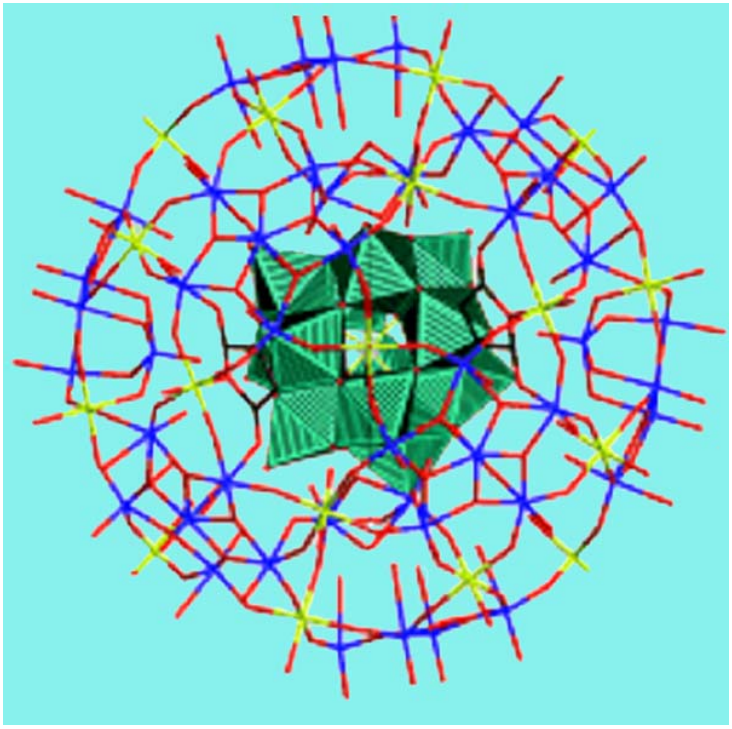

Fig. 2.

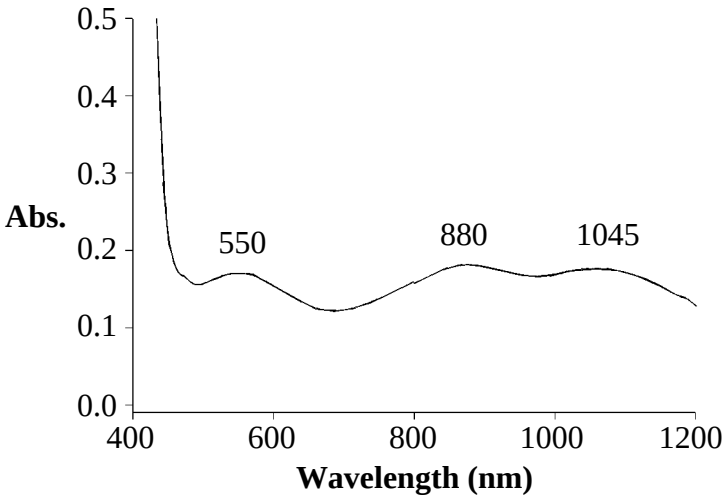
0.5
0.4
0.3
Abs.
0.2
0.1
0.0
550
880
1045
400
600
800
1000
1200
Wavelength (nm)

Fig. 3.

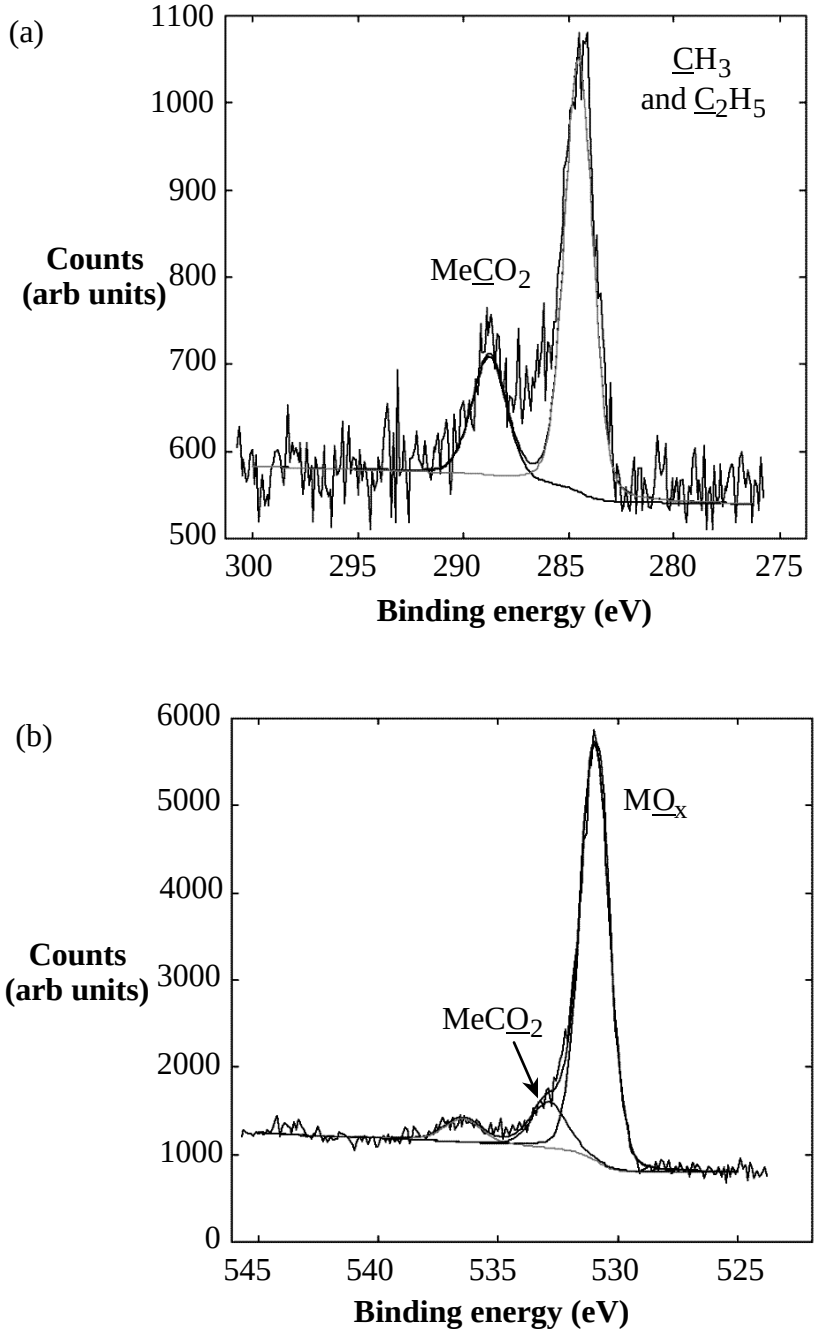
(a)
1100
1000
900
800
700
600
500
Counts
(arb units)
CH3
and C2H5
MeCO2
300
295
290
285
280
275
Binding energy (eV)
(b)
6000
5000
4000
3000
2000
1000
0
Counts
(arb units)
MOx
MeCO2
545
540
535
530
525
Binding energy (eV)

Fig. 4.

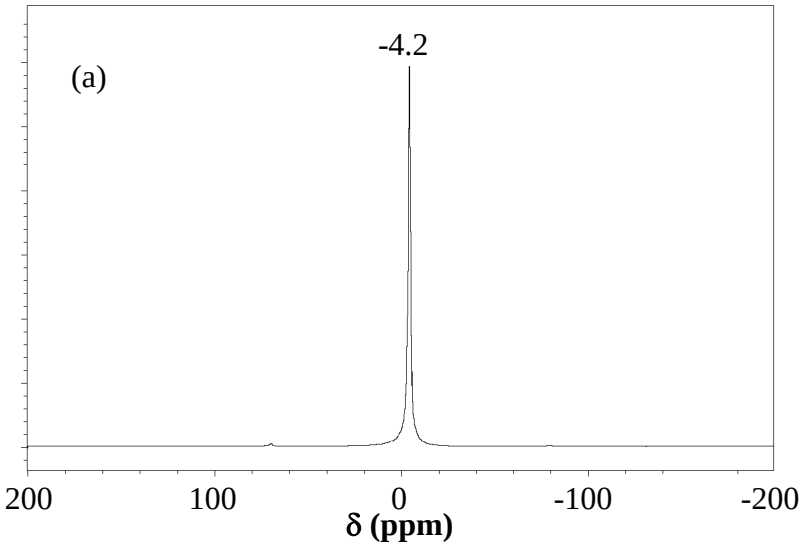

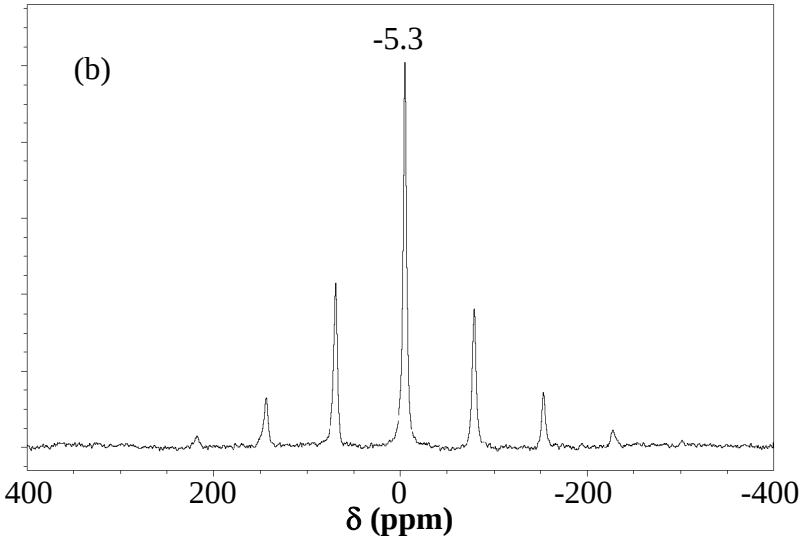

Fig. 5.

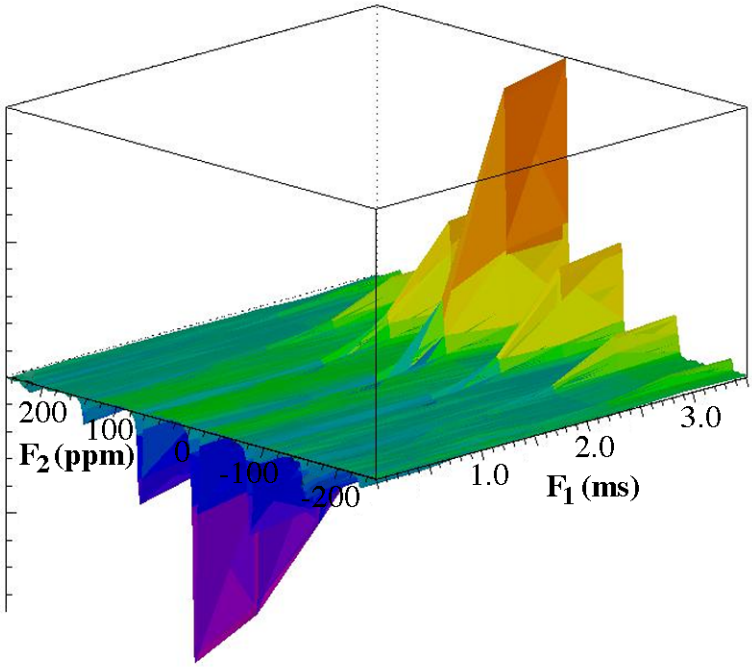

Fig. 6

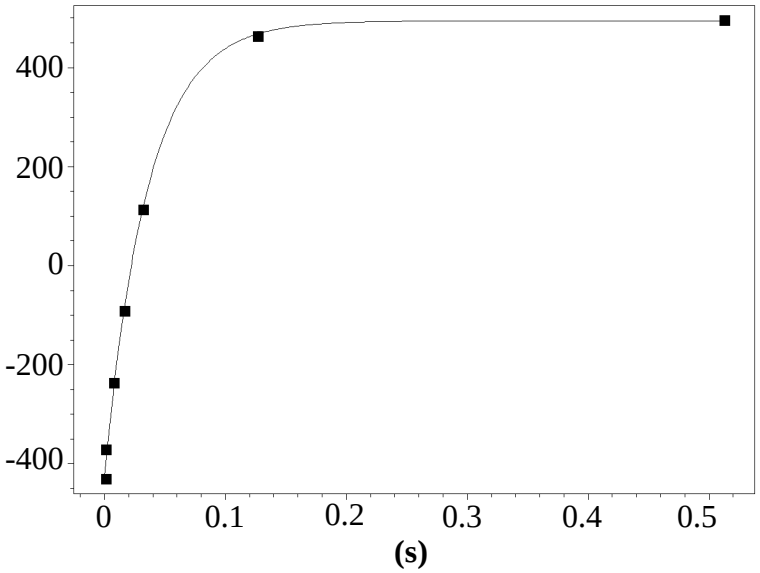

Fig. 7.

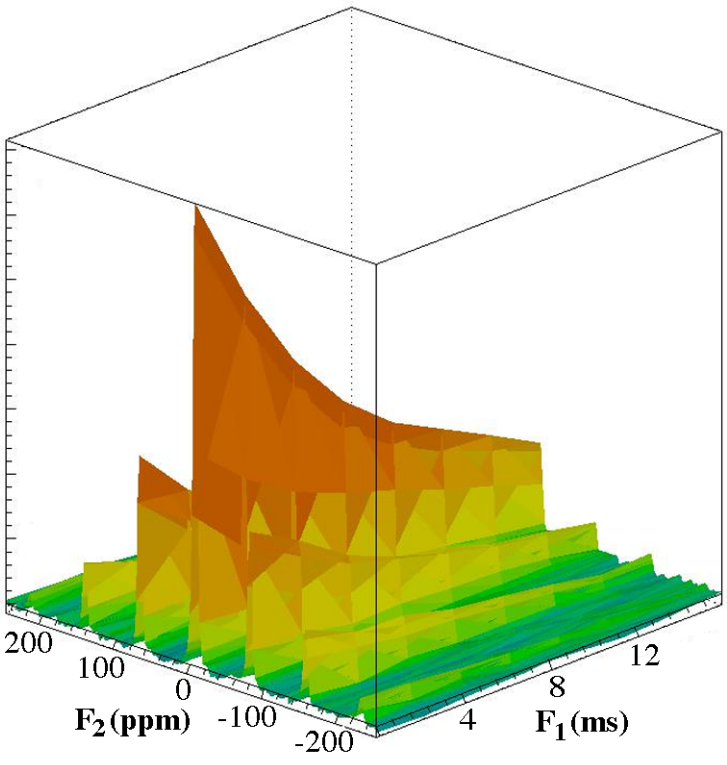

Fig. 8.

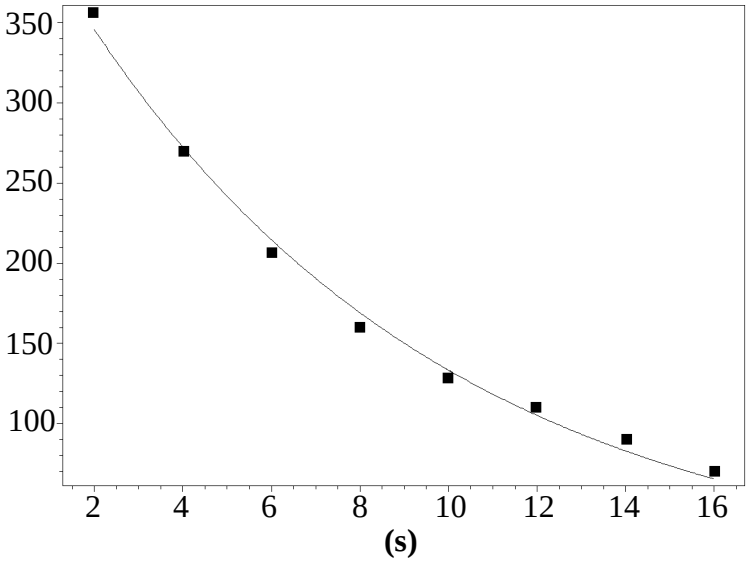

Fig. 9.

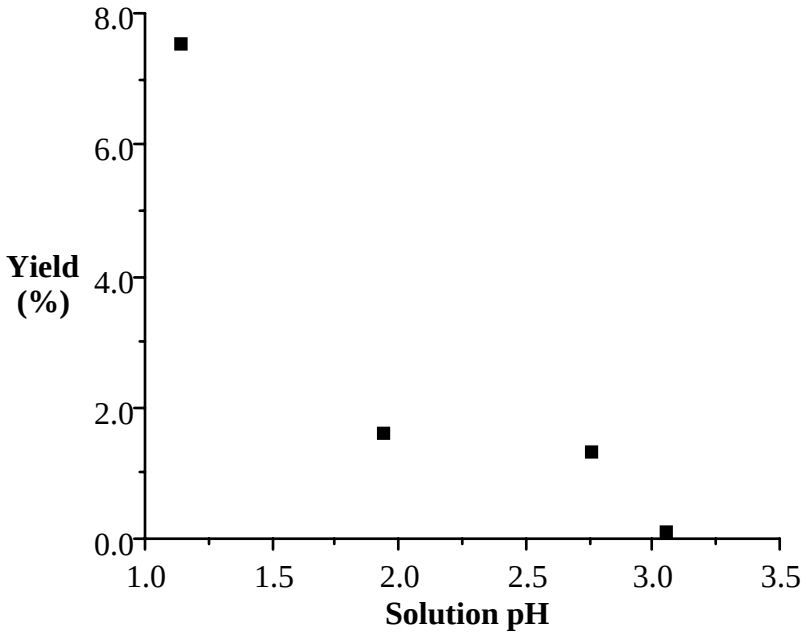

Fig. 10.

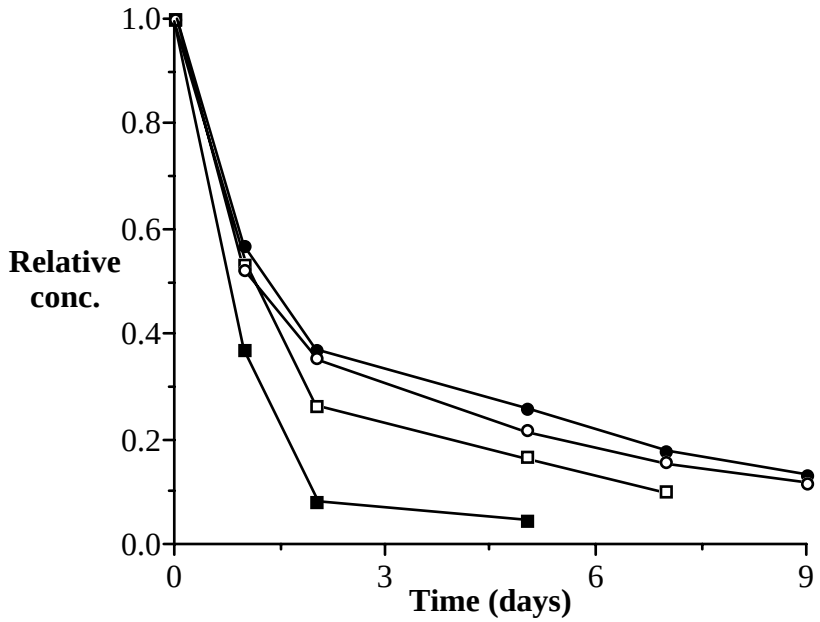

Fig. 11.

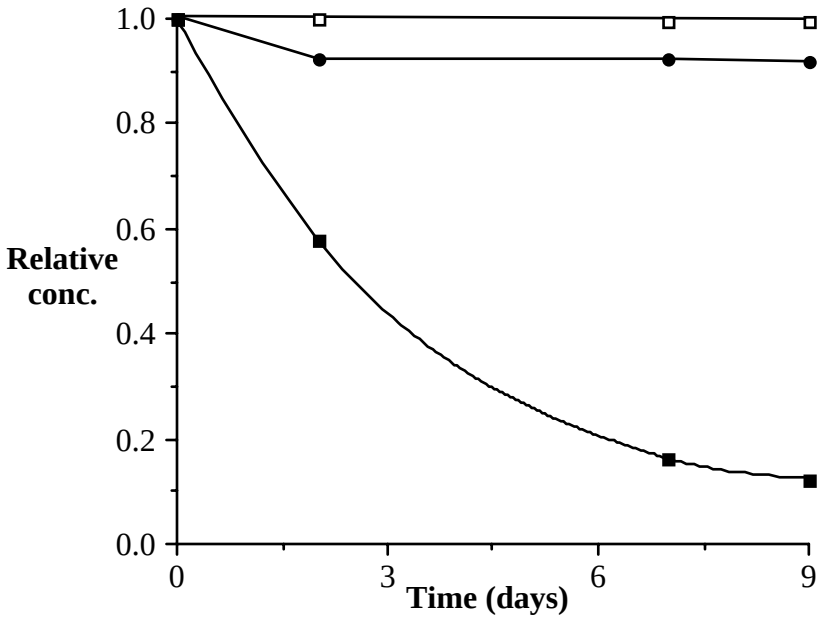

Fig. 12.

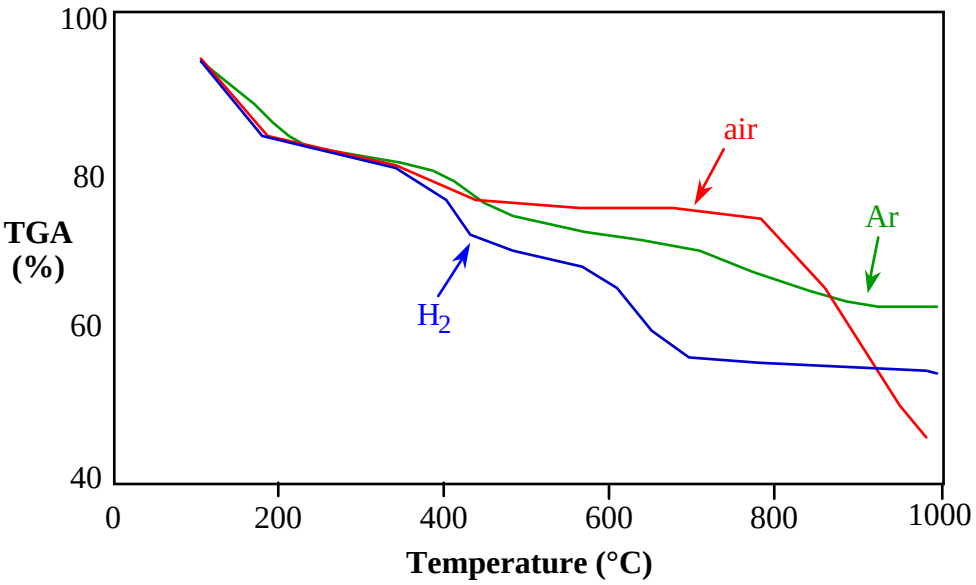

Fig. 13.

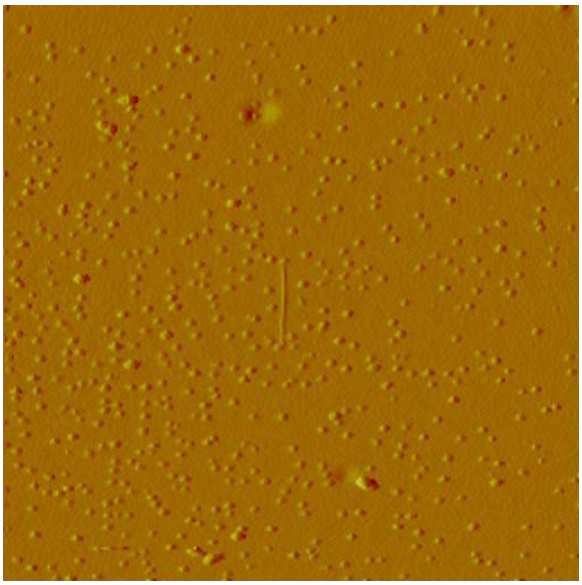

Fig. 14.

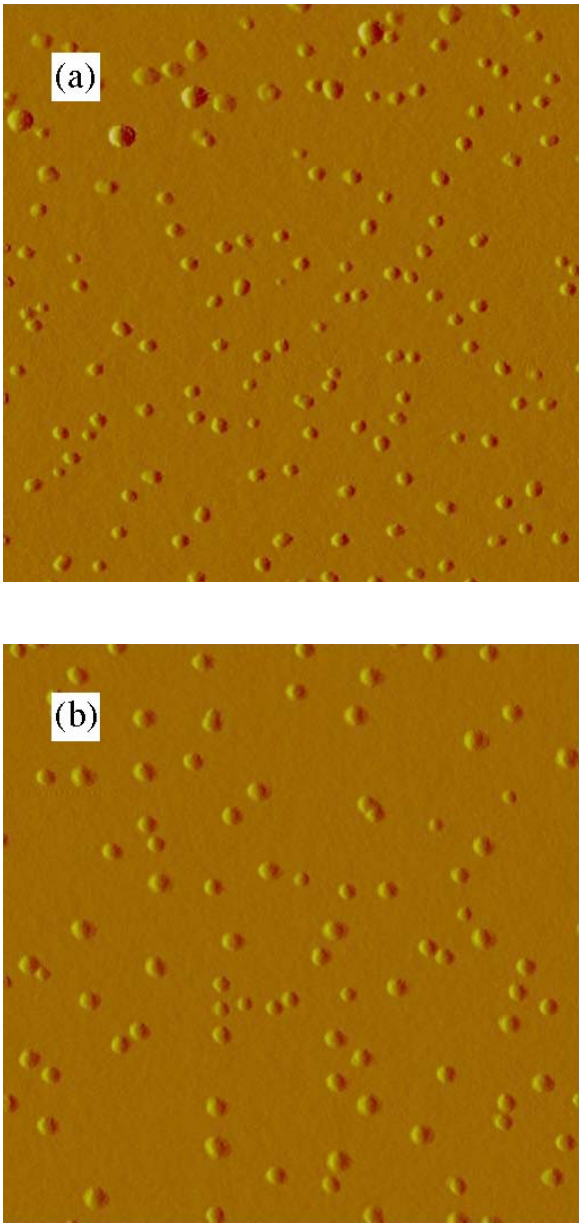

Fig. 14, contd.

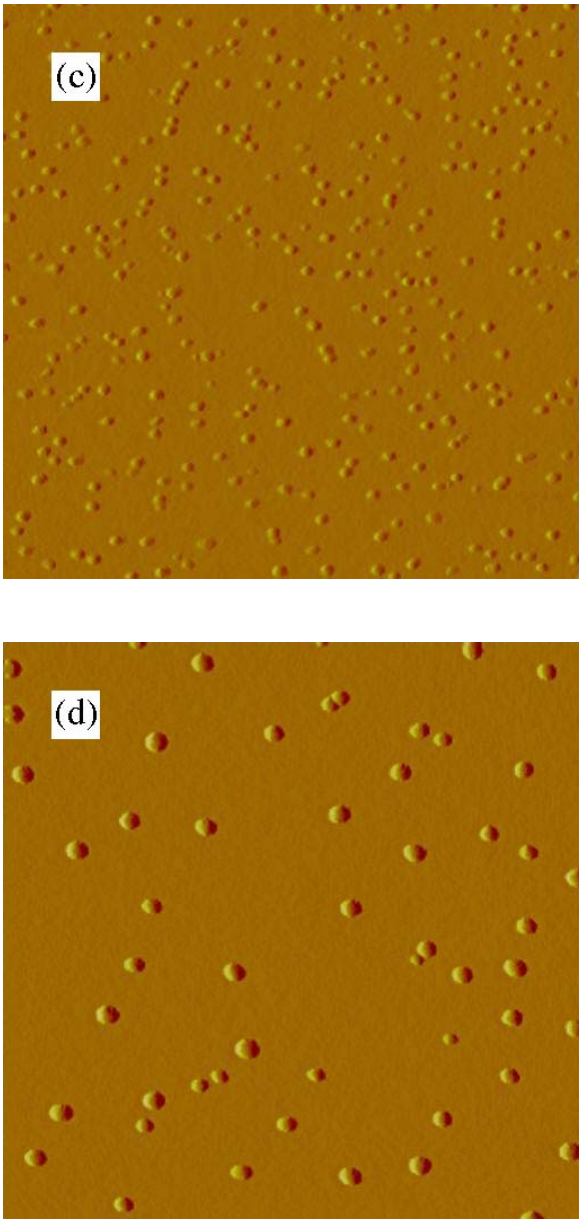

Fig. 15.

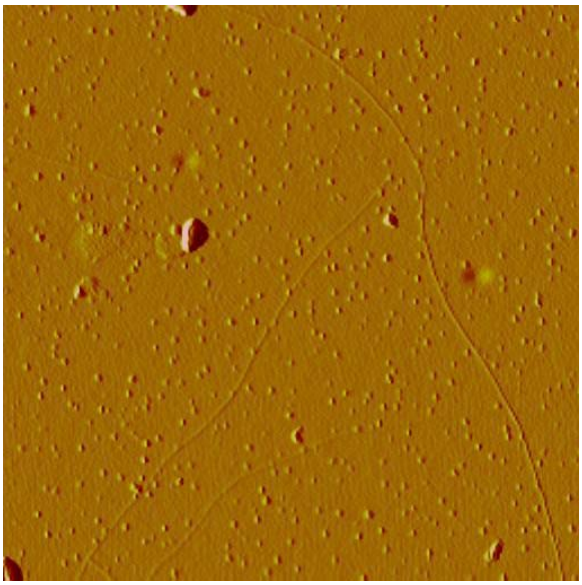

Fig. 16.

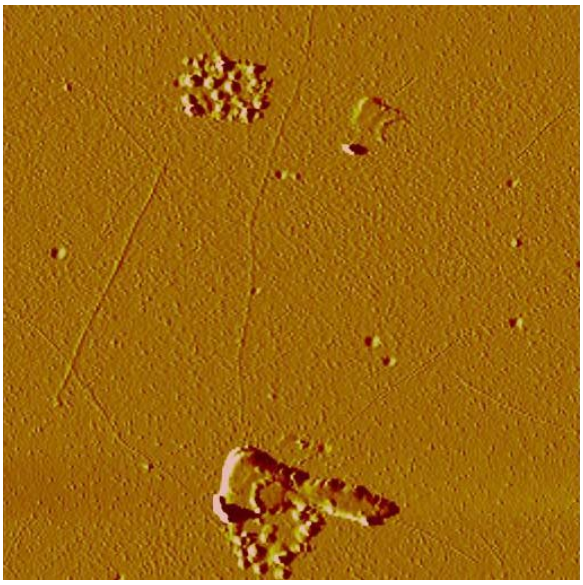

Graphical Abstract

A Study of the Formation, Purification, and Application as a SWNT Growth Catalyst of the Nanocluster $[H_xPMo_{12}O_{40} \subset H_4Mo_{72}Fe_{30}(O_2CMe)_{15}O_{254}(H_2O)_{98}]$

Robin E. Anderson, Ramon Colorado, Jr., Christopher Crouse, Douglas Ogrin, Benji Maruyama, Mark J. Pender, Christopher L. Edwards, Elizabeth Whitsitt, Valerie C. Moore, Dorothy Koveal, Corina Lupu, Michael Stewart, Richard E. Smalley, James M. Tour, and Andrew R. Barron*

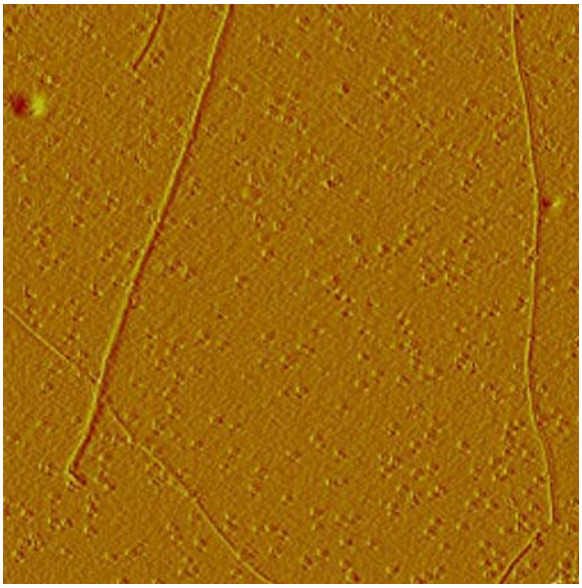

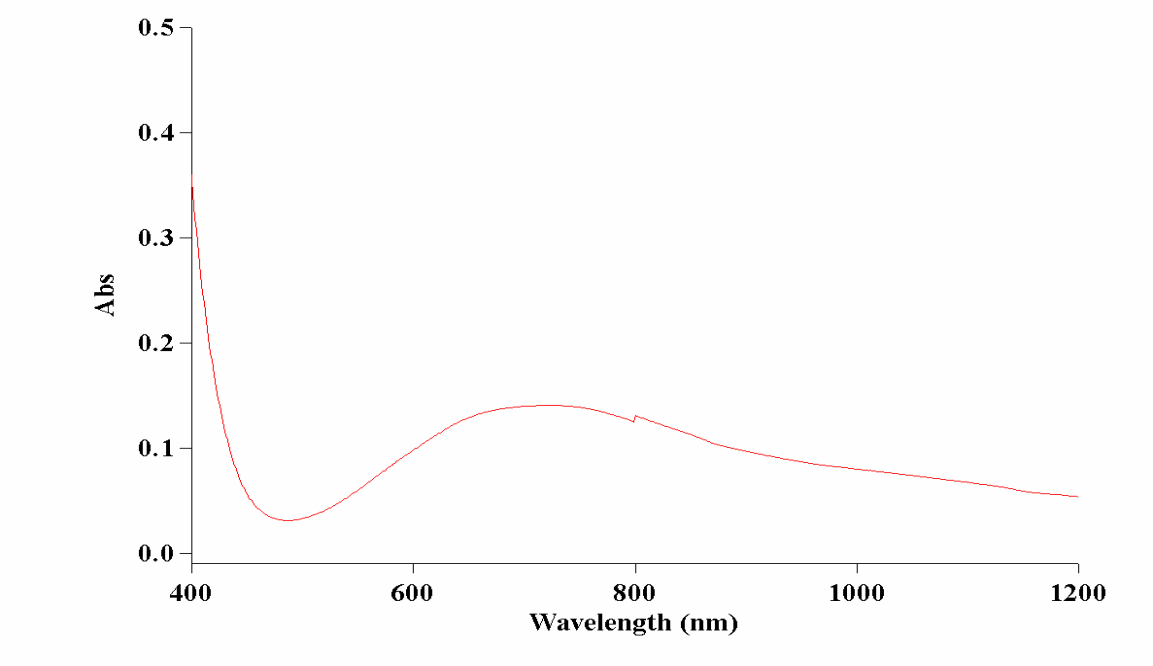

Fig. S1. UV-visible spectrum of the blue water-soluble fraction (in pH 2 water) formed in the synthesis of FeMoC.

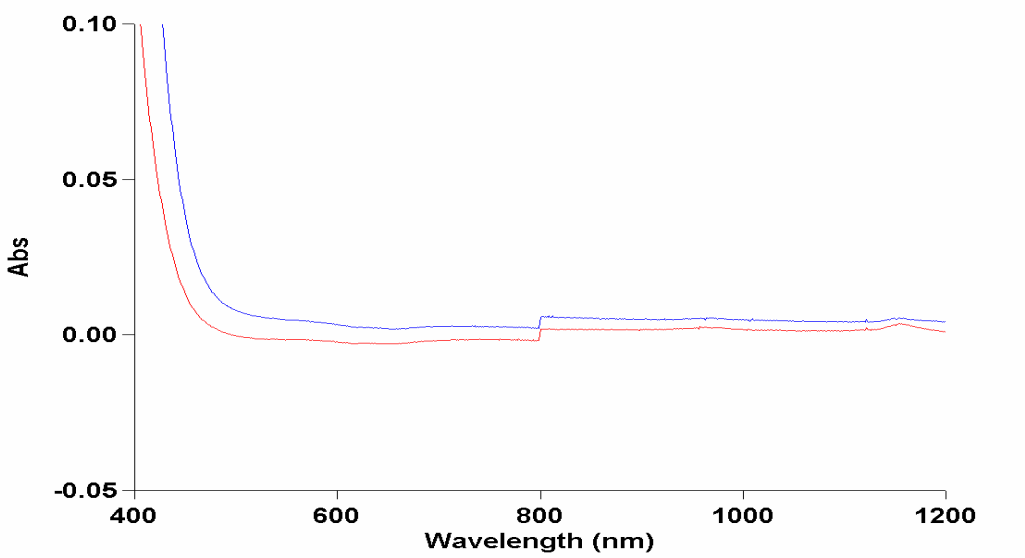

Fig. S2. UV-visible spectra (in H_2O @ pH 2) of the yellow solid formed in the synthesis of FeMoC (red line), and Keplerate (blue line).

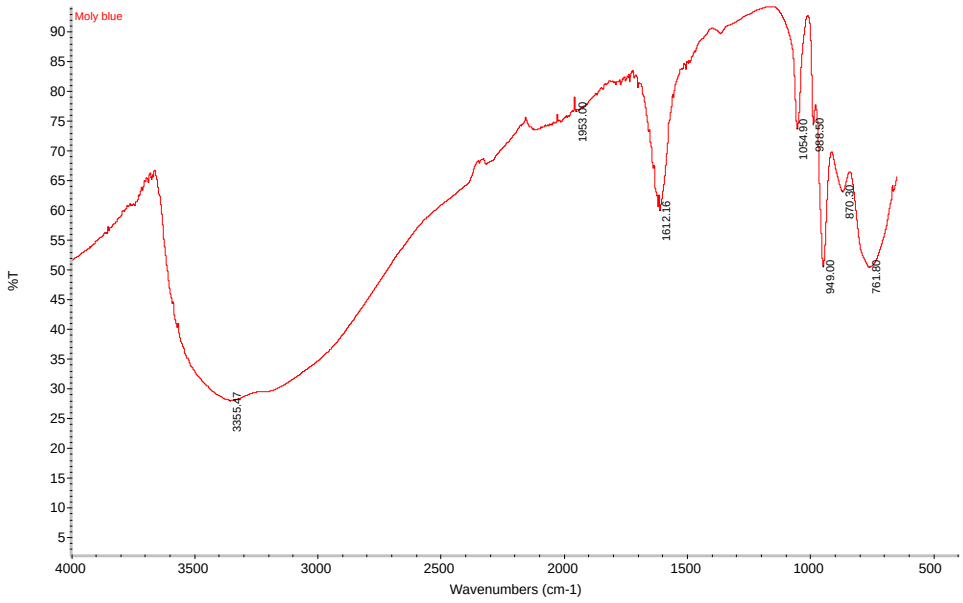

Fig. S3. ATR of the blue fraction formed in the synthesis of FeMoC.

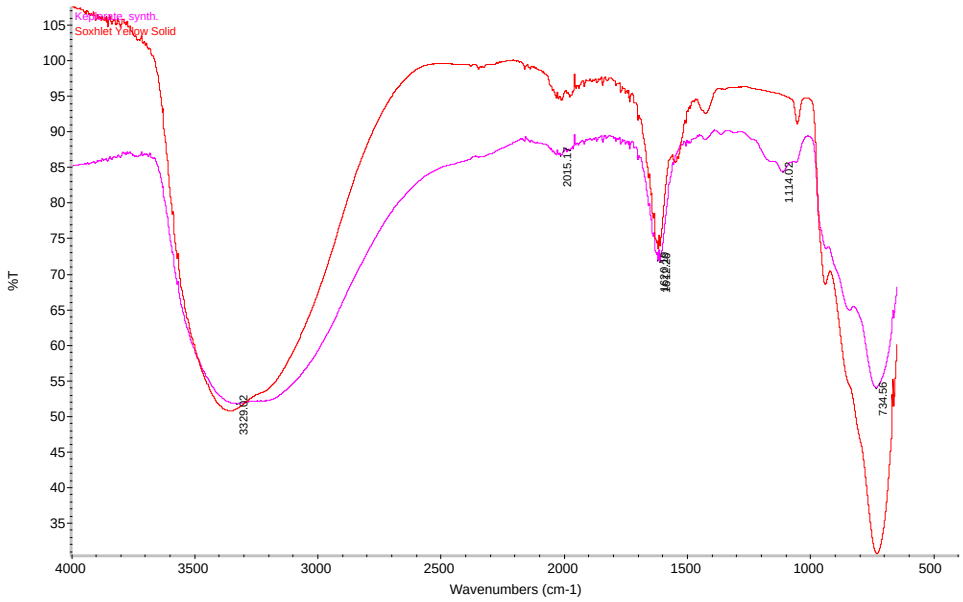

Fig. S4. Comparison of ATR spectra of Keplerate (pink) and the yellow solid (red) formed in the synthesis of FeMoC.

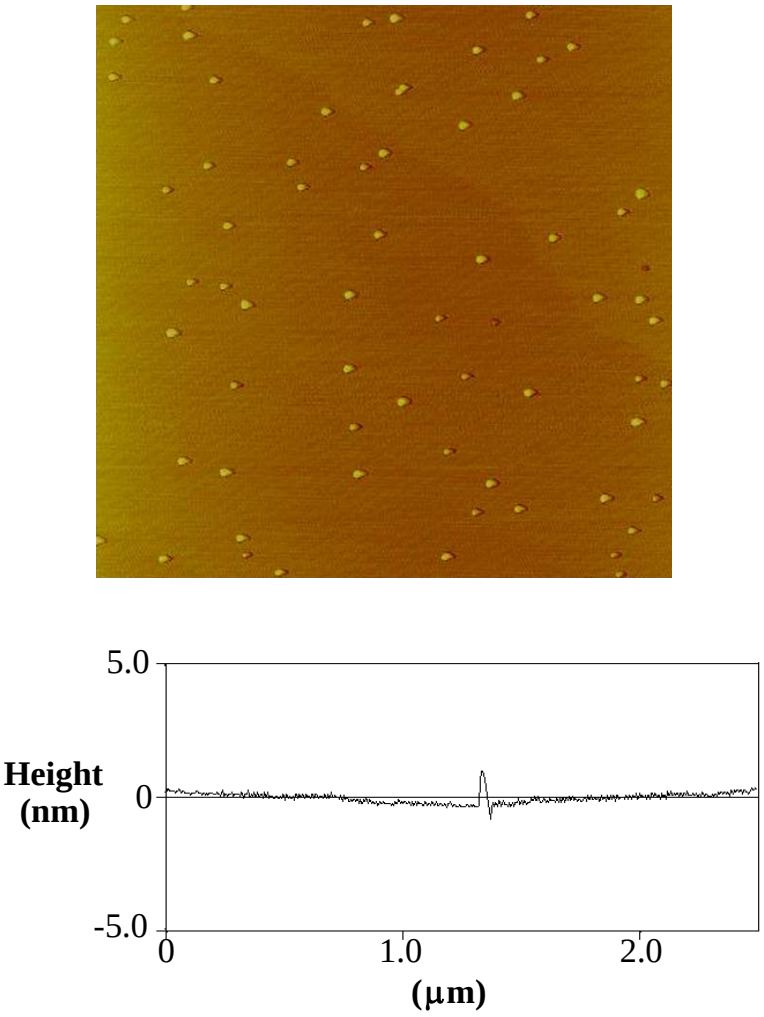

Fig. S5. Representative tapping mode AFM image (2 x 2 μm) and associated height analysis of FeMoC-EtOH showing the features to be about 2 nm tall, the theoretical height is 2.1 nm.

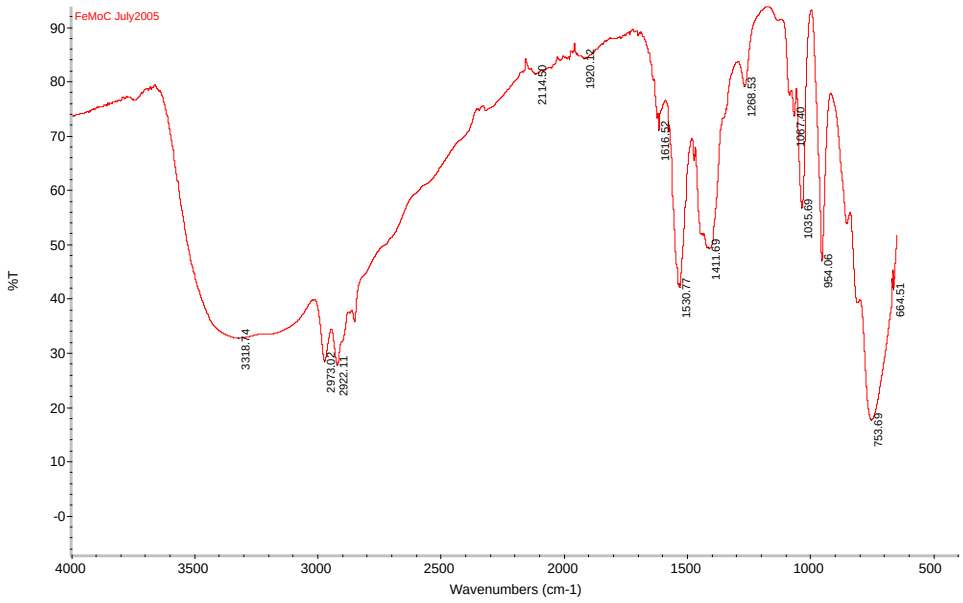

Fig. S6. ATR of FeMoC-EtOH solid.

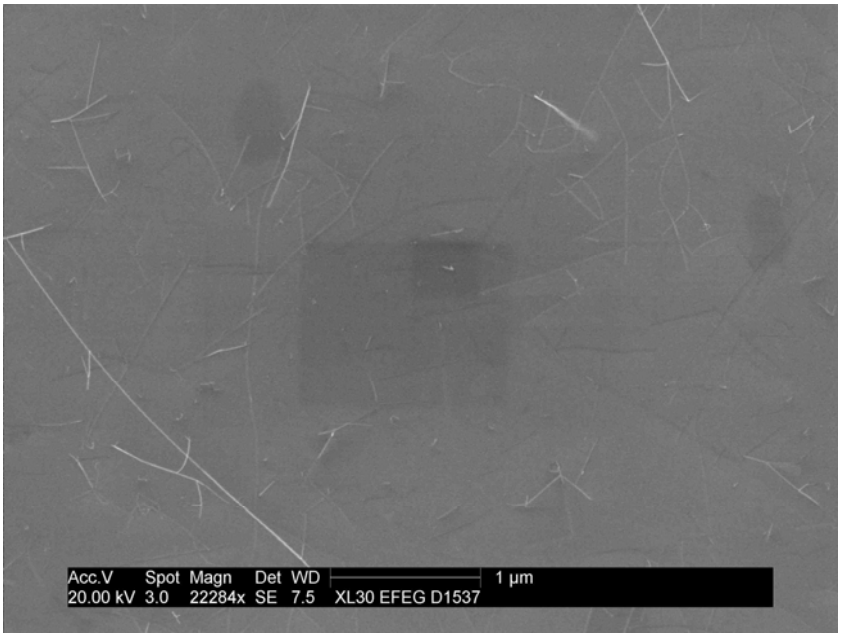

Fig. S7. SEM micrograph of SWNTs grown from aged FeMoC-EtOH on a spin-on-glass surface.

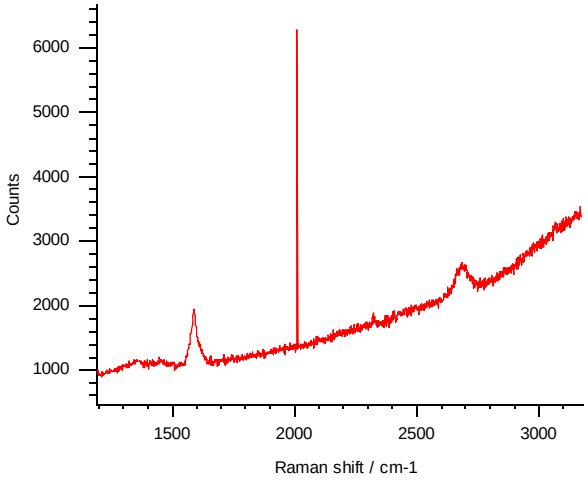

Fig. S8. Raman spectrum of surface after growth run with FeMoC.